

Label-Driven Reconstruction for Domain Adaptation in Semantic Segmentation

Jinyu Yang, Weizhi An, Sheng Wang, Xinliang Zhu, Chaochao Yan, Junzhou Huang
The University of Texas at Arlington

Abstract

Unsupervised domain adaptation enables to alleviate the need for pixel-wise annotation in the semantic segmentation. One of the most common strategies is to translate images from the source domain to the target domain and then align their marginal distributions in the feature space using adversarial learning. However, source-to-target translation enlarges the bias in translated images, owing to the dominant data size of the source domain. Furthermore, consistency of the joint distribution in source and target domains cannot be guaranteed through global feature alignment. Here, we present an innovative framework, designed to mitigate the image translation bias and align cross-domain features with the same category. This is achieved by 1) performing the target-to-source translation and 2) reconstructing both source and target images from their predicted labels. Extensive experiments on adapting from synthetic to real urban scene understanding demonstrate that our framework competes favorably against existing state-of-the-art methods.

1. Introduction

Deep Convolutional Neural Networks (DCNNs) have demonstrated impressive achievements in computer vision tasks, such as image recognition [20], object detection [17], and semantic segmentation [30]. As one of the most fundamental tasks, semantic segmentation predicts pixel-level semantic labels for given images. It plays an extremely important role in autonomous agent applications such as self-driving techniques.

Existing supervised semantic segmentation methods, however, largely rely on pixel-wise annotations which require tremendous time and labor efforts. To overcome this limitation, publicly available synthetic datasets (e.g., GTA [38] and SYNTHIA [39]) which are densely-annotated, have been considered recently. Nevertheless, the most obvious drawback of such a strategy is the poor knowledge generalization caused by domain shift issues (e.g., appearance and spatial layout differences), giving rise to dramatic performance degradation when directly applying models learned from

synthetic data to real-world data of interest. In consequence, domain adaptation has been exploited in recent studies for cross-domain semantic segmentation, where the most common strategy is to learn domain-invariant representations by minimizing distribution discrepancy between source and target domains [50, 27], designing a new loss function [54], considering depth information [7, 46], or alternatively generating pseudo labels and re-training models with these labels through a self-training manner [55, 26]. Following the advances of Generative Adversarial Nets (GAN) [19], adversarial learning has been used to match cross-domain representations by minimizing an adversarial loss on the source and target representations [21, 32, 33, 13], or adapting structured output space across two domains [42, 26]. Recent studies further consider the pixel-level (e.g., texture and lighting) domain shift to enforce source and target images to be domain-invariant in terms of visual appearance [51, 1, 48, 34, 9]. This is achieved by translating images from the source domain to the target domain by using image-to-image translation models such as CycleGAN [53] and UNIT [28].

Despite these painstaking efforts, we are still far from being able to fully adapt cross-domain knowledge mainly stemming from two limitations. First, adversarial-based image-to-image translation introduces inevitable bias to the translated images, as we cannot fully guarantee that the translated source domain $\mathcal{F}(\mathcal{X}_s)$ is identical to the target domain \mathcal{X}_t (\mathcal{X}_s and \mathcal{X}_t denote two domains, and \mathcal{F} indicates an image-to-image translation model). This limitation is especially harmful to the source-to-target translation [51, 1, 48, 34, 26], since the data size of the source domain is much larger than the target domain in most of domain adaptation problems. Second, simply aligning cross-domain representations in the feature space [21, 1, 42] ignores the joint distribution shift (i.e., $\mathcal{P}(G(\mathcal{X}_s), Y_s) \neq \mathcal{P}(G(\mathcal{X}_t), Y_t)$, where G is used for feature extraction, while Y_s and Y_t indicate ground truth labels). These limitations give rise to severe false positive and false negative issues in the target prediction. This problem can get even worse when there is a significant discrepancy in layout or structure between the source and target domains, such as adapting from synthetic to real urban traffic scenes.



Figure 1. An example of our method on synthetic-to-real urban scene adaptation. Given a target-domain (or real) image (a), we first make target-to-source translation to obtain source-like (or synthetic) image (b), and then perform segmentation on these translated images. Our method improves the segmentation accuracy in the target domain by reconstructing both source and target images from their predicted labels (c). (d) illustrates the image reconstructed from (c), while (e) indicates the ground truth label.

In this paper, we propose an innovative domain adaptation framework for semantic segmentation. The key idea is to reduce the image translation bias and align cross-domain feature representations through image reconstruction. As opposed to performing source-to-target translation [1, 48, 26], for the first time, we conduct the target-to-source translation to make target images indistinguishable from source images. This enables to substantially reduce the bias in translated images and allows us to use original source images and their corresponding ground truth to train a segmentation network. Besides, a reconstruction network is designed to reconstruct both source and target images from their predicted labels. It is noteworthy that we reconstruct images directly from the label space, rather than the feature space as reported in previous studies. This is essential to guide the segmentation network by penalizing the reconstructed image that semantically deviates from the corresponding input image. Most importantly, this strategy enforces cross-domain features with the same category close to each other.

The performance of our method is evaluated on synthetic-to-real scenarios of urban scene understanding, i.e., GTA5 to Cityscapes and SYNTHIA to Cityscapes. Our results demonstrate that the proposed method achieves significant improvements compared with existing methods. Figure 1 demonstrates an example of our model in adapting cross-domain knowledge in semantic segmentation tasks and reconstructing the input image from its output label. We also carry out comprehensive ablation studies to analyze the effectiveness of each component in our framework.

The contribution of this paper is threefold.

- For the first time, we propose and investigate the target-to-source translation in domain adaptation. It enables the reduction of the image translation bias compared to the widely-used source-to-target translation.
- To enforce semantic consistency, we introduce a label-driven reconstruction module that reconstructs both source and target images from their predicted labels.
- Extensive experiments show that our method achieves the new state-of-the-art performance on adapting synthetic-to-real semantic segmentation.

2. Related Work

Semantic Segmentation Recent achievements in semantic segmentation mainly benefit from the technical advances of DCNNs, especially the emergence of Fully Convolutional Network (FCN) [30]. By adapting and extending contemporary deep classification architectures fully convolutionally, FCN enables pixel-wise semantic prediction for any arbitrary-sized inputs and has been widely recognized as one of the benchmark methods in this field. Numerous methods inspired by FCN were then proposed to further enhance segmentation accuracy, which have exhibited distinct performance improvement on the well-known datasets (e.g., PASCAL VOC 2012 [14] and Cityscapes [11]) [5, 29, 52, 6, 4].

However, such methods heavily rely on human-annotated, pixel-level segmentation masks, which require extremely expensive labeling efforts [11]. In consequence, weakly-supervised methods, which are based on easily obtained annotations (e.g., bounding boxes and image-level tags), were proposed to alleviate the need for effort-consuming labeling [12, 37]. Another alternative is to resort to freely-available synthetic datasets (e.g., GTA5 [38] and SYNTHIA [39]) with pixel-level semantic annotations. However, models learned on synthetic datasets suffer from significant performance degradation when directly applied to the real datasets of interest, mainly owing to the domain shift issue.

Domain Adaptation Domain adaptation aims to mitigate the domain discrepancy between a source and a target domain, which can be further divided into supervised adaptation, semi-supervised adaptation, and unsupervised adaptation, depending on the availability of labels in the target domain. The term unsupervised domain adaptation refers to the scenario where target labels are unavailable and have been extensively studied [31, 45, 15, 43, 44, 49].

Recent publications have highlighted the complementary role of pixel-level and representation-level adaptation in semantic segmentation [1, 35, 51, 48, 7], where the pixel-level adaptation is mainly achieved by translating images from the source domain to the target domain (source-to-target translation). Specifically, unpaired image-to-image translation is used in CyCADA [1] to achieve pixel-level adaptation by restricting cycle-consistency. Similarly, FCAN achieves

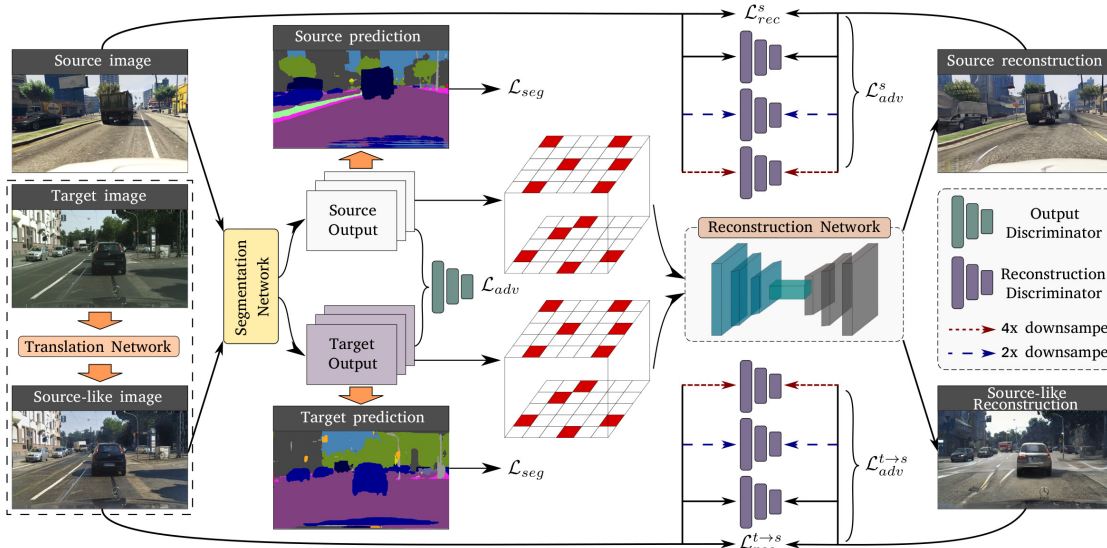


Figure 3. Schematic overview of our framework which has three modules: (i) a translation network for pixel-level discrepancy reduction by translating target images to source-like images, where source-like images are indistinguishable from source images, (ii) a segmentation network that predicts segmentation outputs for source images and source-like images, and (iii) a reconstruction network for reconstructing source and source-like images from their corresponding label space.



Figure 4. A comparison between the image reconstruction from feature space and label space (ours). For each input image (first column), the first and second row indicate the images reconstructed from the feature and label space, respectively.

ported in previous domain adaptation methods, we conduct the target-to-source translation through an unsupervised image translation network (Figure 3). Our goal is to learn a mapping $\mathcal{F} : \mathcal{X}_t \rightarrow \mathcal{X}_s$ such that the distribution of images from $\mathcal{F}(\mathcal{X}_t)$ is indistinguishable from the distribution of \mathcal{X}_s . As a counterpart, the inverse mapping $\mathcal{F}^{-1} : \mathcal{X}_s \rightarrow \mathcal{X}_t$, which maps images from \mathcal{X}_s to \mathcal{X}_t , is introduced to prevent the mode collapse issue [18]. Two adversarial discriminators \mathcal{D}_t and \mathcal{D}_s are employed for distribution match, where \mathcal{D}_t enforces indistinguishable distribution between $\mathcal{F}(\mathcal{X}_t)$ and \mathcal{X}_s , and \mathcal{D}_s encourages indistinguishable distribution between $\mathcal{F}^{-1}(\mathcal{X}_s)$ and \mathcal{X}_t (More details can be found in the **Supplementary**).

Based on the trained model \mathcal{F} , we first translate images from \mathcal{X}_t to source-like images $\mathcal{X}_{t \rightarrow s} = \mathcal{F}(\mathcal{X}_t)$. Specifically, each image in $\mathcal{X}_{t \rightarrow s}$ preserves the same content as the corresponding image in \mathcal{X}_t while demonstrating the common style (e.g., texture and lighting) as \mathcal{X}_s . \mathcal{X}_s and $\mathcal{X}_{t \rightarrow s}$ are then fed into a segmentation network for semantic label prediction.

Compared to translating images from the source domain to the target domain, the target-to-source translation has two benefits. First, it allows full supervision on the source domain by training the segmentation network with original source images and their corresponding labels. Second, it enables to reduce the bias in translated images, given that $|\mathcal{X}_t| \ll |\mathcal{X}_s|$.

3.3. Semantic Segmentation

Given that source-like images $\mathcal{X}_{t \rightarrow s}$ preserves all semantic information from \mathcal{X}_t , we apply a shared segmentation network G to \mathcal{X}_s and $\mathcal{X}_{t \rightarrow s}$ to predict their segmentation outputs with the loss function given by,

$$\mathcal{L}_G = \mathcal{L}_{seg}(G(\mathcal{X}_s), Y_s) + \mathcal{L}_{seg}(G(\mathcal{X}_{t \rightarrow s}), Y_t^{ssl}) + \lambda \mathcal{L}_{adv}(G(\mathcal{X}_s), G(\mathcal{X}_{t \rightarrow s})), \quad (1)$$

where \mathcal{L}_{seg} indicates the typical segmentation objective, Y_t^{ssl} is pseudo labels of $\mathcal{X}_{t \rightarrow s}$ which is derived from [26], $\mathcal{L}_{adv}(G(\mathcal{X}_s), G(\mathcal{X}_{t \rightarrow s}))$ is an adversarial loss, and λ leverages the importance of these losses. Specifically,

Table 1. A performance comparison of our method with other state-of-the-art models on "GTA5 to Cityscapes". The performance is measured by the intersection-over-union (IoU) for each class, mean IoU (mIoU), and mIoU gap between each model and the fully-supervised model (Oracle). Two base architectures, i.e., VGG16 (V) and ResNet101 (R) are used in our study.

		GTA5 → Cityscapes																						
	Base	road	sidewalk	building	wall	fence	pole	traffic light	traffic sign	vegetation	terrain	sky	person	rider	car	truck	bus	train	motorbike	bicycle	mIoU	mIoU Gap	Oracle	
Source only	R	75.8	16.8	77.2	12.5	21.0	25.5	30.1	20.1	81.3	24.6	70.3	53.8	26.4	49.9	17.2	25.9	6.5	25.3	36.0	36.6	-28.5	65.1	
SIBAN [32]	R	88.5	35.4	79.5	26.3	24.3	28.5	32.5	18.3	81.2	40.0	76.5	58.1	25.8	82.6	30.3	34.4	3.4	21.6	21.5	42.6	-22.5	65.1	
CLAN [33]	R	87.0	27.1	79.6	27.3	23.3	28.3	35.5	24.2	83.6	27.4	74.2	58.6	28.0	76.2	33.1	36.7	6.7	31.9	31.4	43.2	-21.9	65.1	
DISE [3]	R	91.5	47.5	82.5	31.3	25.6	33.0	33.7	25.8	82.7	28.8	82.7	62.4	30.8	85.2	27.7	34.5	6.4	25.2	24.4	45.4	-19.7	65.1	
BDL [26]	R	91.0	44.7	84.2	34.6	27.6	30.2	36.0	36.0	85.0	43.6	83.0	58.6	31.6	83.3	35.3	49.7	3.3	28.8	35.6	48.5	-16.6	65.1	
Ours	R	90.8	41.4	84.7	35.1	27.5	31.2	38.0	32.8	85.6	42.1	84.9	59.6	34.4	85.0	42.8	52.7	3.4	30.9	38.1	49.5	-15.6	65.1	
Source only	V	26.0	14.9	65.1	5.5	12.9	8.9	6.0	2.5	70.0	2.9	47.0	24.5	0.0	40.0	12.1	1.5	0.0	0.0	0.0	17.9	-46.7	64.6	
SIBAN [32]	V	83.4	13.0	77.8	20.4	17.5	24.6	22.8	9.6	81.3	29.6	77.3	42.7	10.9	76.0	22.8	17.9	5.7	14.2	2.0	34.2	-26.1	60.3	
AdaptSegNet [42]	V	87.3	29.8	78.6	21.1	18.2	22.5	21.5	11.0	79.7	29.6	71.3	46.8	6.5	80.1	23.0	26.9	0.0	10.6	0.3	35.0	-25.2	61.8	
CyCADA [1]	V	85.2	37.2	76.5	21.8	15.0	23.8	22.9	21.5	80.5	31.3	60.7	50.5	9.0	76.9	17.1	28.2	4.5	9.8	0.0	35.4	-24.9	60.3	
CLAN [33]	V	88.0	30.6	79.2	23.4	20.5	26.1	23.0	14.8	81.6	34.5	72.0	45.8	7.9	80.5	26.6	29.9	0.0	10.7	0.0	36.6	-23.7	60.3	
CrDoCo [9]	V	89.1	33.2	80.1	26.9	25.0	18.3	23.4	12.8	77.0	29.1	72.4	55.1	20.2	79.9	22.3	19.5	1.0	20.1	18.7	38.1	-22.2	60.3	
BDL [26]	V	89.2	40.9	81.2	29.1	19.2	14.2	29.0	19.6	83.7	35.9	80.7	54.7	23.3	82.7	25.8	28.0	2.3	25.7	19.9	41.3	-19.0	60.3	
Ours	V	90.1	41.2	82.2	30.3	21.3	18.3	33.5	23.0	84.1	37.5	81.4	54.2	24.3	83.0	27.6	32.0	8.1	29.7	26.9	43.6	-16.8	60.3	

$\mathcal{L}_{adv}(G(\mathcal{X}_s), G(\mathcal{X}_{t \rightarrow s}))$ is defined as,

$$\mathcal{L}_{adv}(G(\mathcal{X}_s), G(\mathcal{X}_{t \rightarrow s})) = \mathbb{E}[\log D(G(\mathcal{X}_s))] + \mathbb{E}[\log(1 - D(G(\mathcal{X}_{t \rightarrow s})))] \quad (2)$$

which enforces G to learn domain-invariant features by confusing the discriminator D . It is noteworthy that we regard the segmentation outputs $G(\mathcal{X}_s)$ and $G(\mathcal{X}_{t \rightarrow s})$ as features in our study. This is based on the observation that \mathcal{X}_s and $\mathcal{X}_{t \rightarrow s}$ share significant similarities in terms of spatial layouts and structures [42].

3.4. Image Reconstruction from the Label Space

To encourage G to generate segmentation outputs that are semantic consistent, we introduce a reconstruction network \mathcal{M} to reconstruct \mathcal{X}_ϕ from $G(\mathcal{X}_\phi) \in \mathbb{R}^{H_\phi \times W_\phi \times C}$, where (H_ϕ, W_ϕ) indicates image size, C represents the number of label classes, and the subscript ϕ can be either s or $t \rightarrow s$ to denote the source or the target domain. However, directly reconstructing images from the feature space fails to provide semantic consistency constraint to G . On the one hand, $G(\mathcal{X}_\phi)$ encodes rich information which makes the image reconstruction quite straightforward. As illustrated in Figure 4, in just a few epochs, the reconstructed images derived from \mathcal{M} are almost identical to the input images. On the other hand, to enforce cross-domain features with the same category close to each other, it is essential to perform the reconstruction based on the label space. Unfortunately, $G(\mathcal{X}_\phi)$ lies in the feature space instead. To overcome these limitations, the most clear-cut way is to convert $G(\mathcal{X}_\phi)$ to have zeros everywhere except where the index of each maximum

value in the last dimension. Doing so formulates the categorical representation of the predicted label that corresponds to $G(\mathcal{X}_\phi)$. Nevertheless, such conversion is non-differentiable and cannot be trained using standard backpropagation.

Driven by the softmax action selection which is commonly used in the reinforcement learning, we apply Boltzmann distributed probabilities to approximate the semantic label map of $G(\mathcal{X}_\phi)$, which is defined as,

$$\Omega_\phi^{(h,w,i)} = \frac{\exp(G(\mathcal{X}_\phi)^{(h,w,i)} / \tau)}{\sum_{j=1}^c \exp(G(\mathcal{X}_\phi)^{(h,w,j)} / \tau)} \quad (3)$$

where τ is a temperature parameter. This conversion is continuous and differentiable, therefore, we use \mathcal{M} to reconstruct input images \mathcal{X}_ϕ from Ω_ϕ (Figure 4).

To synthesize high-resolution images from the semantic label map, we use conditional GANs [22] to model the conditional distribution of \mathcal{X}_ϕ given Ω_ϕ . To this end, we introduce \mathcal{M} and multi-scale domain discriminators D_k for $k = 1, 2, 3$. \mathcal{M} is designed to reconstruct \mathcal{X}_ϕ from Ω_ϕ , and D_k aims to distinguish \mathcal{X}_ϕ from $\mathcal{M}(\Omega_\phi)$. Specifically, \mathcal{M} follows the architecture proposed in [23], while D_k is based on PatchGAN [22] that penalizes structure at the scale of image patches. All D_k follow the same network architecture. Besides \mathcal{X}_ϕ and $\mathcal{M}(\Omega_\phi)$ themselves, they are downsampled by a factor of 2 and 4 to obtain pyramid of 3 scales for D_1 , D_2 , and D_3 , respectively. It is worth mentioning that D_k is essential to differentiate real and reconstructed images with high resolution [47], owing to its ability in providing large

Table 2. A performance comparison of our method with other state-of-the-art models on "SYNTHIA to Cityscapes". The performance is measured by the IoU for each class, mIoU, and mIoU gap between each model and the fully-supervised model (Oracle). Two base architectures, i.e., VGG16 (V) and ResNet101 (R) are used in our study.

		SYNTHIA → Cityscapes																	mIoU	mIoU Gap	Oracle
	Base	road	sidewalk	building	wall	fence	pole	traffic light	traffic sign	vegetation	sky	person	rider	car	bus	motorbike	bicycle				
Source only	R	55.6	23.8	74.6	—	—	—	6.1	12.1	74.8	79.0	55.3	19.1	39.6	23.3	13.7	25.0	38.6	—	—	
AdaptSegNet [42]	R	84.3	42.7	77.5	—	—	—	4.7	7.0	77.9	82.5	54.3	21.0	72.3	32.2	18.9	32.3	46.7	-25.0	71.7	
DISE [3]	R	91.7	53.5	77.1	—	—	—	6.2	7.6	78.4	81.2	55.8	19.2	82.3	30.3	17.1	34.3	48.8	-22.9	71.7	
DADA [46]	R	89.2	44.8	81.4	—	—	—	8.6	11.1	81.8	84.0	54.7	19.3	79.7	40.7	14.0	38.8	49.8	-21.9	71.7	
BDL [26]	R	86.0	46.7	80.3	—	—	—	14.1	11.6	79.2	81.3	54.1	27.9	73.7	42.2	25.7	45.3	51.4	-20.3	71.7	
Ours	R	85.1	44.5	81.0	—	—	—	16.4	15.2	80.1	84.8	59.4	31.9	73.2	41.0	32.6	44.7	53.1	-18.6	71.7	
ROAD-Net [8]	V	77.7	30.0	77.5	9.6	0.3	25.8	10.3	15.6	77.6	79.8	44.5	16.6	67.8	14.5	7.0	23.8	36.2	-27.6	64.1	
SPiGAN [25]	V	71.1	29.8	71.4	3.7	0.3	33.2	6.4	15.6	81.2	78.9	52.7	13.1	75.9	25.5	10.0	20.5	36.8	-22.7	59.5	
GIO-Ada [7]	V	78.3	29.2	76.9	11.4	0.3	26.5	10.8	17.2	81.7	81.9	45.8	15.4	68.0	15.9	7.5	30.4	37.3	-26.8	64.1	
TGCF-DA [10]	V	90.1	48.6	80.7	2.2	0.2	27.2	3.2	14.3	82.1	78.4	54.4	16.4	82.5	12.3	1.7	21.8	38.5	-25.6	64.1	
BDL [26]	V	72.0	30.3	74.5	0.1	0.3	24.6	10.2	25.2	80.5	80.0	54.7	23.2	72.7	24.0	7.5	44.9	39.0	-20.5	59.5	
Ours	V	73.7	29.6	77.6	1.0	0.4	26.0	14.7	26.6	80.6	81.8	57.2	24.5	76.1	27.6	13.6	46.6	41.1	-18.4	59.5	

receptive field. The objective function is given by,

$$\mathcal{L}_{adv}^{\phi} = \sum_{k=1}^3 [\mathbb{E}[\log D_k(\Omega_{\phi}, \mathcal{X}_{\phi})] + \mathbb{E}[\log(1 - D_k(\Omega_{\phi}, \mathcal{M}(\Omega_{\phi})))]] \quad (4)$$

To further enforce semantic consistency between \mathcal{X}_{ϕ} and $\mathcal{M}(\Omega_{\phi})$, we introduce a cycle-reconstruction loss \mathcal{L}_{rec}^{ϕ} to match their feature representations, which is defined as,

$$\mathcal{L}_{rec}^{\phi} = \mathbb{E} \sum_{m=1}^M [||V^{(m)}(\mathcal{M}(\Omega_{\phi})) - V^{(m)}(\mathcal{X}_{\phi})||_1] + \mathbb{E} \sum_{k=1}^3 \sum_{n=1}^N [||D_k^{(n)}(\Omega_{\phi}, \mathcal{X}_{\phi}) - D_k^{(n)}(\Omega_{\phi}, \mathcal{M}(\Omega_{\phi}))||_1] \quad (5)$$

where V is a VGG19-based model for extracting high-level perceptual information [23], M and N represent the total number of layers in V and D_k for matching intermediate representations. Note that \mathcal{L}_{rec}^{ϕ} penalizes Ω_{ϕ} when it deviates from the corresponding image \mathcal{X}_{ϕ} in terms of semantic consistency. In this way, \mathcal{M} enables to map features from $\mathcal{X}_{t \rightarrow s}$ closer to the features from \mathcal{X}_s with the same label.

Taken together, the training objective of our framework is formulated as,

$$\min_{G, \mathcal{M}} \max_{D_1, D_2, D_3} \mathcal{L}_G + \alpha(\mathcal{L}_{adv}^s + \mathcal{L}_{adv}^{t \rightarrow s}) + \beta(\mathcal{L}_{rec}^s + \mathcal{L}_{rec}^{t \rightarrow s}) \quad (6)$$

where α and β leverage the importance of losses above. Notably, our method is able to implicitly encourage G to generate semantic-consistent segmentation labels for the target domain.

4. Experiments

In this section, a comprehensive evaluation is performed on two domain adaption tasks to assess our framework for semantic segmentation. Specifically, we consider the large distribution shift of adapting from synthetic (i.e., GTA5 [38] and SYNTHIA [39]) to the real images in Cityscapes [11]. A thorough comparison with the state-of-the-art methods and extensive ablation studies are also carried out to verify the effectiveness of each component in our framework.

4.1. Datasets

Cityscapes is one of the benchmarks for urban scene understanding, which is collected from 50 cities with varying scene layouts and weather conditions. The 5,000 finely-annotated images from this dataset are used in our study, which contains 2,975 training images, 500 validation images, and 1,525 test images. Each image with a resolution of 2048×1024 . The GTA5 dataset is synthesized from the game Grand Theft Auto V (GTA5), including a total of 24,966 labeled images whose annotations are compatible with Cityscapes. The resolution of each image is 1914×1052 . The SYNTHIA-RAND-CITYSCAPES (or SYNTHIA for short) contains 9,400 pixel-level annotated images (1280×760), which are synthesized from a virtual city. Following the same setting reported in the previous studies, we use the labeled SYNTHIA or GTA5 dataset as the source domain, while using the unlabeled training dataset in the CITYSCAPES as the target domain. Only the 500 labeled validation images from CITYSCAPES are used as test data in all of our experiments.

Table 3. Ablation study on GTA5 \rightarrow Cityscapes. S \rightarrow T and T \rightarrow S indicate source-to-target and target-to-source translation.

Base	S \rightarrow T	T \rightarrow S	Reconstruction	mIoU
R	✓			48.5
R		✓		49.1
R		✓	✓	49.5
V	✓			41.3
V		✓		42.3
V		✓	✓	43.6

4.2. Network Architecture

We use two segmentation baseline models, i.e., FCN-VGG16 and DeepLab-ResNet101 to investigate the effectiveness and generalizability of our framework. Specifically, FCN-VGG16 is the combination of FCN-8s [30] and VGG16 [41], while DeepLab-ResNet101 is obtained by integrating DeepLab-V2 [6] into ResNet101 [20]. These two segmentation models share the same discriminator which has 5 convolution layers with channel number 64, 128, 256, 512, 1. For each layer, a leaky ReLU parameterized by 0.2 is followed, except the last one. The kernel size and stride are set to 4×4 and 2, respectively. The reconstruction model follows the architecture in [23], containing 3 convolution layers (kernel 3×3 and stride 1), 9 ResNet blocks (kernel 3×3 and stride 2), and another 3 transposed convolution layers (kernel 3×3 and stride 2) for upsampling. The 3 multi-scale discriminators share the identical network, each of which follows the architecture of PatchGAN [22]. More details regarding the architecture of discriminators in both segmentation and reconstruction models can be found in the **Supplementary**.

4.3. Implementation Details

Our framework is implemented with PyTorch [36] on two TITAN Xp GPUs, each of which with 12GB memory. The batch size is set to one for training all the models discussed below. Limited by the GPU memory space, the translation network is first trained to perform target-to-source image translation by using Adam optimizer [24]. The initial learning rate is set to 0.0001, which is reduced by half after every 100,000 iterations. We use momentum {0.5, 0.999} with weight decay 0.0001. The maximum training iteration is $1000k$.

DeepLab-ResNet101 is trained using Stochastic Gradient Descent optimizer with initial learning rate 2.5×10^{-4} . The polynomial decay with power 0.9 is applied to the learning rate. The momentum and weight decay are set to 0.9 and 5×10^{-4} , respectively. For FCN-VGG16, the Adam optimizer with momentum {0.9, 0.99} and initial learning rate 1×10^{-5} is used for training. The learning rate is decreased using step decay with step size 50000 and drop factor 0.1. In equation 1, λ is set to 1×10^{-3} for DeepLab-ResNet101 and 1×10^{-4} for FCN-VGG16.

The reconstruction network is first pre-trained by recon-

Table 4. Ablation study on SYNTHIA \rightarrow Cityscapes. S \rightarrow T and T \rightarrow S indicate source-to-target and target-to-source translation.

Base	S \rightarrow T	T \rightarrow S	Reconstruction	mIoU
R	✓			51.4
R		✓		52.0
R		✓	✓	53.1
V	✓			39.0
V		✓		40.1
V		✓	✓	41.1

structing source images \mathcal{X}_s from the corresponding labels Y_s . We use the Adam optimizer with initial learning rate 2×10^{-4} and momentum {0.5, 0.999}, where the learning rate is linearly decreased to zero. In equation 6, we set $\beta = 10$. α is set to 0.01 and 0.001 for FCN-VGG16 and DeepLab-ResNet101 respectively.

4.4. GTA5 \rightarrow Cityscapes

We carry out the adaptation from GTA5 to Cityscapes by following the same evaluation protocol as previously reported in [42, 26]. The overall quantitative performance is assessed on 19 common classes (e.g., road, wall, and car) between these two domains. As shown in Table 1, we achieve the best performance compared to existing state-of-the-art methods in this field. Specifically, our method surpasses the source-only model (without adaptation) by 12.9% and 25.7% on ResNet101 and VGG16, respectively. Compared with CyCADA [1] and BDL [26] that rely on source-to-target translation, we demonstrate significant improvements (i.e., 8.2% and 2.3% on VGG16) by reducing image translation bias. CLAN [33] aims to enforce local semantic consistency by a category-level adversarial network. However, such a strategy fails to account for the global semantic consistency. Our reconstruction network shares a similar spirit with CLAN in terms of joint distribution alignment but enables to enforce semantic consistency from a global view. As a consequence, we get 6.3% and 7.0% improvement on ResNet101 and VGG16, respectively. We further investigate our model’s ability in narrowing the mIoU gap between the model (Oracle) that is trained in a fully-supervised matter. The results demonstrate that we significantly recover the performance loss caused by the domain shift issue.

4.5. SYNTHIA \rightarrow Cityscapes

We then evaluate our framework on the adaptation from SYNTHIA to Cityscapes based on 13 classes on ResNet101 and 16 classes on VGG16. The results exhibit that our method outperforms other competing methods on average as shown in Table 2. Both AdaptSegNet [42] and BDL [26] adapt output space in their models. However, simply aligning segmentation outputs may lead to negative transfer issue, owing to the dramatic differences of the layout and structure between SYNTHIA and Cityscapes. We achieve

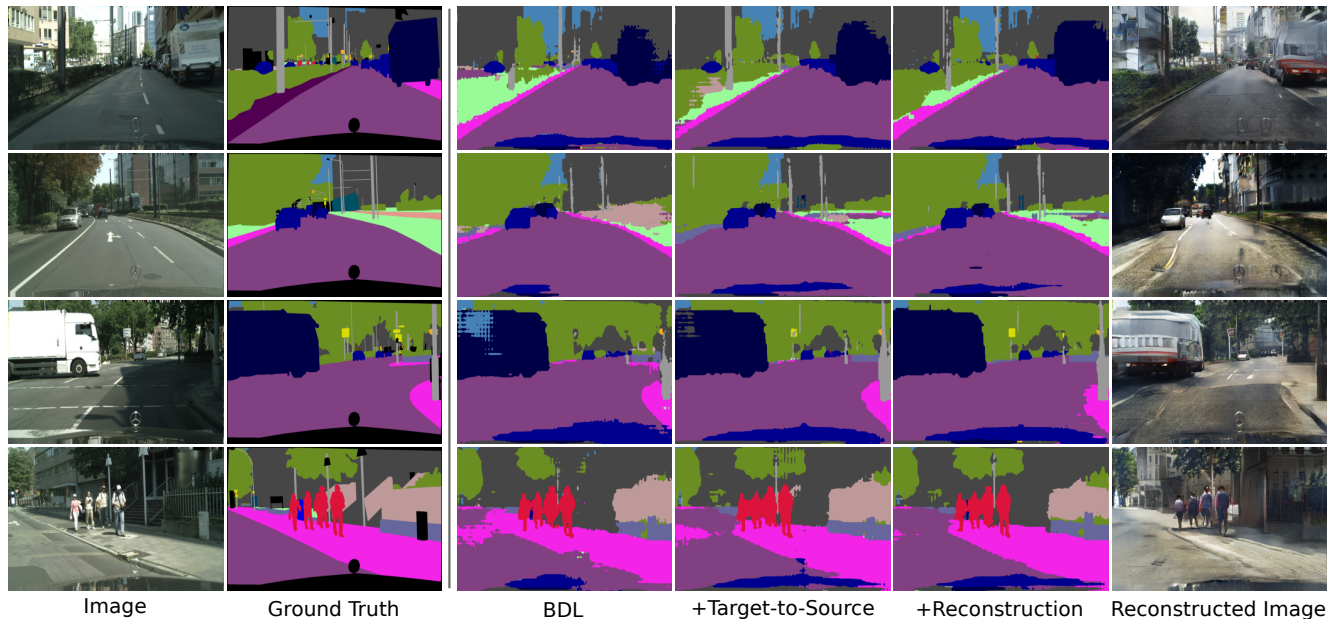


Figure 5. Qualitative examples of semantic segmentation results in Cityscapes. For each target-domain image (first column), its ground truth and the corresponding segmentation prediction from the baseline model are given. The following are predictions of our method by incorporating target-to-source translation and reconstruction, together with the reconstructed image.

6.4% and 1.7% improvement than AdaptSegNet and BDL on ResNet101, respectively. Besides, our method narrows down the mIoU gap between the oracle model by a large margin.

4.6. Ablation Study

GTA5 \rightarrow Cityscapes Compared to the baseline model, 0.6% improvement is achieved by considering target-to-source translation on ResNet101 (Table 3). By further enforce semantic consistency through a reconstruction network, our method achieves 49.5 mIoU. Similar improvements are also observed on VGG16, with 1.0% improvement over the baseline by performing target-to-source translation. The prediction power of our method is further boosted by combining translation and reconstruction, giving rise to another 1.3% mIoU improvement. The qualitative study of each module in our method is showcased in Figure 5.

SYNTIA \rightarrow Cityscapes We achieve a performance boost of 0.6% and 1.1% over the baseline by considering image translation on ResNet101 and VGG16, respectively (Table 4). The performance gain is 1.1% and 1.0% by incorporating the reconstruction network. Our results prove the effectiveness of target-to-source translation and reconstruction in adapting domain knowledge for semantic segmentation.

Parameter Analysis We investigate the sensitivity of temperature parameter τ in this section and find that $\tau = 0.001$

Table 5. Ablation study of the temperature τ on GTA5 \rightarrow Cityscapes.

τ	0.0001	0.001	0.01	0.1	1
mIoU	42.7	43.6	42.8	42.9	41.5

achieves the best performance (Table 5). Therefore, τ is set to 0.001 in all of our experiments to approximate semantic label maps.

5. Conclusion

We propose a novel framework that exploits cross-domain adaptation in the context of semantic segmentation. Specifically, we translate images from a target domain to a source domain to reduce image translation bias. To enforce cross-domain features with the same category close to each other, we reconstruct both source and target images directly from the label space. Experiments demonstrate that our method achieves significant improvement in adapting from GTA5 and SYNTIA to Cityscapes.

References

- [1] Cycada: Cycle consistent adversarial domain adaptation. In *International Conference on Machine Learning (ICML)*, 2018. 1, 2, 5, 7
- [2] Konstantinos Bousmalis, George Trigeorgis, Nathan Silberman, Dilip Krishnan, and Dumitru Erhan. Domain separation networks. In *Advances in neural information processing systems (NIPS)*, pages 343–351, 2016. 3

- [3] Wei-Lun Chang, Hui-Po Wang, Wen-Hsiao Peng, and Wei-Chen Chiu. All about structure: Adapting structural information across domains for boosting semantic segmentation. In *Proceedings of the IEEE Conference on Computer Vision and Pattern Recognition (CVPR)*, pages 1900–1909, 2019. 3, 5, 6
- [4] Liang-Chieh Chen, Maxwell D Collins, Yukun Zhu, George Papandreou, Barret Zoph, Florian Schroff, Hartwig Adam, and Jonathon Shlens. Searching for efficient multi-scale architectures for dense image prediction. In *Advances in neural information processing systems (NIPS)*, 2018. 2
- [5] Liang-Chieh Chen, George Papandreou, Iasonas Kokkinos, Kevin Murphy, and Alan L Yuille. Semantic image segmentation with deep convolutional nets and fully connected crfs. In *International Conference on Learning Representations (ICLR)*, 2014. 2
- [6] Liang-Chieh Chen, George Papandreou, Iasonas Kokkinos, Kevin Murphy, and Alan L Yuille. Deeplab: Semantic image segmentation with deep convolutional nets, atrous convolution, and fully connected crfs. *IEEE transactions on pattern analysis and machine intelligence (TPAMI)*, 40(4):834–848, 2018. 2, 7
- [7] Yuhua Chen, Wen Li, Xiaoran Chen, and Luc Van Gool. Learning semantic segmentation from synthetic data: A geometrically guided input-output adaptation approach. In *Proceedings of the IEEE Conference on Computer Vision and Pattern Recognition (CVPR)*, pages 1841–1850, 2019. 1, 2, 3, 6
- [8] Yuhua Chen, Wen Li, and Luc Van Gool. Road: Reality oriented adaptation for semantic segmentation of urban scenes. In *Proceedings of the IEEE Conference on Computer Vision and Pattern Recognition (CVPR)*, pages 7892–7901, 2018. 6
- [9] Yun-Chun Chen, Yen-Yu Lin, Ming-Hsuan Yang, and Jia-Bin Huang. Crdoco: Pixel-level domain transfer with cross-domain consistency. In *Proceedings of the IEEE Conference on Computer Vision and Pattern Recognition (CVPR)*, pages 1791–1800, 2019. 1, 5
- [10] Jaehoon Choi, Taekyung Kim, and Changick Kim. Self-ensembling with gan-based data augmentation for domain adaptation in semantic segmentation. In *Proceedings of the IEEE international conference on computer vision (ICCV)*, 2019. 6
- [11] Marius Cordts, Mohamed Omran, Sebastian Ramos, Timo Rehfeld, Markus Enzweiler, Rodrigo Benenson, Uwe Franke, Stefan Roth, and Bernt Schiele. The cityscapes dataset for semantic urban scene understanding. In *Proceedings of the IEEE Conference on Computer Vision and Pattern Recognition (CVPR)*, pages 3213–3223, 2016. 2, 6
- [12] Jifeng Dai, Kaiming He, and Jian Sun. Boxesup: Exploiting bounding boxes to supervise convolutional networks for semantic segmentation. In *Proceedings of the IEEE international conference on computer vision (ICCV)*, pages 1635–1643, 2015. 2
- [13] Liang Du, Jingang Tan, Hongye Yang, Jianfeng Feng, Xiangyang Xue, Qibao Zheng, Xiaoqing Ye, and Xiaolin Zhang. Ssf-dan: Separated semantic feature based domain adaptation network for semantic segmentation. In *Proceedings of the IEEE international conference on computer vision (ICCV)*, 2019. 1
- [14] M. Everingham, L. Van Gool, C. K. I. Williams, J. Winn, and A. Zisserman. The PASCAL Visual Object Classes Challenge 2012 (VOC2012) Results. <http://www.pascal-network.org/challenges/VOC/voc2012/workshop/index.html>. 2
- [15] Yaroslav Ganin and Victor Lempitsky. Unsupervised domain adaptation by backpropagation. In *International Conference on Machine Learning (ICML)*, 2015. 2
- [16] Muhammad Ghifary, W Bastiaan Kleijn, Mengjie Zhang, David Balduzzi, and Wen Li. Deep reconstruction-classification networks for unsupervised domain adaptation. In *Proceedings of the European Conference on Computer Vision (ECCV)*, pages 597–613, 2016. 3
- [17] Ross Girshick. Fast r-cnn. In *Proceedings of the IEEE international conference on computer vision (ICCV)*, pages 1440–1448, 2015. 1
- [18] Ian Goodfellow. Nips 2016 tutorial: Generative adversarial networks. *arXiv preprint arXiv:1701.00160*, 2016. 4
- [19] Ian Goodfellow, Jean Pouget-Abadie, Mehdi Mirza, Bing Xu, David Warde-Farley, Sherjil Ozair, Aaron Courville, and Yoshua Bengio. Generative adversarial nets. In *Advances in neural information processing systems (NIPS)*, pages 2672–2680, 2014. 1
- [20] Kaiming He, Xiangyu Zhang, Shaoqing Ren, and Jian Sun. Deep residual learning for image recognition. In *Proceedings of the IEEE Conference on Computer Vision and Pattern Recognition (CVPR)*, pages 770–778, 2016. 1, 7
- [21] Judy Hoffman, Dequan Wang, Fisher Yu, and Trevor Darrell. Fcns in the wild: Pixel-level adversarial and constraint-based adaptation. *arXiv preprint arXiv:1612.02649*, 2016. 1
- [22] Phillip Isola, Jun-Yan Zhu, Tinghui Zhou, and Alexei A Efros. Image-to-image translation with conditional adversarial networks. In *Proceedings of the IEEE Conference on Computer Vision and Pattern Recognition (CVPR)*, pages 1125–1134, 2017. 5, 7
- [23] Justin Johnson, Alexandre Alahi, and Li Fei-Fei. Perceptual losses for real-time style transfer and super-resolution. In *Proceedings of the European Conference on Computer Vision (ECCV)*, pages 694–711, 2016. 5, 6, 7
- [24] Diederik P Kingma and Jimmy Ba. Adam: A method for stochastic optimization. In *International Conference on Learning Representations (ICLR)*, 2014. 7
- [25] Kuan-Hui Lee, German Ros, Jie Li, and Adrien Gaidon. Spigan: Privileged adversarial learning from simulation. In *International Conference on Learning Representations (ICLR)*, 2019. 6
- [26] Yunsheng Li, Lu Yuan, and Nuno Vasconcelos. Bidirectional learning for domain adaptation of semantic segmentation. In *Proceedings of the IEEE Conference on Computer Vision and Pattern Recognition (CVPR)*, 2019. 1, 2, 3, 4, 5, 6, 7
- [27] Qing Lian, Fengmao Lv, Lixin Duan, and Boqing Gong. Constructing self-motivated pyramid curriculums for cross-domain semantic segmentation: A non-adversarial approach. In *Proceedings of the IEEE international conference on computer vision (ICCV)*, 2019. 1
- [28] Ming-Yu Liu, Thomas Breuel, and Jan Kautz. Unsupervised image-to-image translation networks. In *Advances in neural*

- information processing systems (NIPS)*, pages 700–708, 2017. [1](#)
- [29] Ziwei Liu, Xiao Xiao Li, Ping Luo, Chen-Change Loy, and Xiaoou Tang. Semantic image segmentation via deep parsing network. In *Proceedings of the IEEE international conference on computer vision (ICCV)*, pages 1377–1385, 2015. [2](#)
- [30] Jonathan Long, Evan Shelhamer, and Trevor Darrell. Fully convolutional networks for semantic segmentation. In *Proceedings of the IEEE Conference on Computer Vision and Pattern Recognition (CVPR)*, pages 3431–3440, 2015. [1](#), [2](#), [7](#)
- [31] Mingsheng Long, Yue Cao, Jianmin Wang, and Michael I Jordan. Learning transferable features with deep adaptation networks. In *International Conference on Machine Learning (ICML)*, 2015. [2](#)
- [32] Yawei Luo, Ping Liu, Tao Guan, Junqing Yu, and Yi Yang. Significance-aware information bottleneck for domain adaptive semantic segmentation. In *Proceedings of the IEEE international conference on computer vision (ICCV)*, October 2019. [1](#), [5](#)
- [33] Yawei Luo, Liang Zheng, Tao Guan, Junqing Yu, and Yi Yang. Taking a closer look at domain shift: Category-level adversaries for semantics consistent domain adaptation. In *Proceedings of the IEEE Conference on Computer Vision and Pattern Recognition (CVPR)*, pages 2507–2516, 2019. [1](#), [5](#), [7](#)
- [34] Zak Murez, Soheil Kolouri, David Kriegman, Ravi Ramamoorthi, and Kyunghyun Kim. Image to image translation for domain adaptation. In *Proceedings of the IEEE Conference on Computer Vision and Pattern Recognition (CVPR)*, pages 4500–4509, 2018. [1](#)
- [35] Zak Murez, Soheil Kolouri, David Kriegman, Ravi Ramamoorthi, and Kyunghyun Kim. Image to image translation for domain adaptation. In *Proceedings of the IEEE Conference on Computer Vision and Pattern Recognition (CVPR)*, volume 13, 2018. [2](#), [3](#)
- [36] Adam Paszke, Sam Gross, Soumith Chintala, Gregory Chanan, Edward Yang, Zachary DeVito, Zeming Lin, Alban Desmaison, Luca Antiga, and Adam Lerer. Automatic differentiation in pytorch. 2017. [7](#)
- [37] Pedro O Pinheiro and Ronan Collobert. From image-level to pixel-level labeling with convolutional networks. In *Proceedings of the IEEE Conference on Computer Vision and Pattern Recognition (CVPR)*, pages 1713–1721, 2015. [2](#)
- [38] Stephan R Richter, Vibhav Vineet, Stefan Roth, and Vladlen Koltun. Playing for data: Ground truth from computer games. In *Proceedings of the European Conference on Computer Vision (ECCV)*, pages 102–118, 2016. [1](#), [2](#), [6](#)
- [39] German Ros, Laura Sellart, Joanna Materzynska, David Vazquez, and Antonio M Lopez. The synthia dataset: A large collection of synthetic images for semantic segmentation of urban scenes. In *Proceedings of the IEEE Conference on Computer Vision and Pattern Recognition (CVPR)*, pages 3234–3243, 2016. [1](#), [2](#), [6](#)
- [40] Swami Sankaranarayanan, Yogesh Balaji, Arpit Jain, Ser Nam Lim, and Rama Chellappa. Learning from synthetic data: Addressing domain shift for semantic segmentation. In *Proceedings of the IEEE Conference on Computer Vision and Pattern Recognition (CVPR)*, 2018. [3](#)
- [41] Karen Simonyan and Andrew Zisserman. Very deep convolutional networks for large-scale image recognition. In *International Conference on Learning Representations (ICLR)*, 2015. [7](#)
- [42] Yi-Hsuan Tsai, Wei-Chih Hung, Samuel Schulter, Kihyuk Sohn, Ming-Hsuan Yang, and Manmohan Chandraker. Learning to adapt structured output space for semantic segmentation. In *Proceedings of the IEEE Conference on Computer Vision and Pattern Recognition (CVPR)*, 2018. [1](#), [3](#), [5](#), [6](#), [7](#)
- [43] Eric Tzeng, Judy Hoffman, Trevor Darrell, and Kate Saenko. Simultaneous deep transfer across domains and tasks. In *Proceedings of the IEEE international conference on computer vision (ICCV)*, pages 4068–4076, 2015. [2](#)
- [44] Eric Tzeng, Judy Hoffman, Kate Saenko, and Trevor Darrell. Adversarial discriminative domain adaptation. In *Proceedings of the IEEE Conference on Computer Vision and Pattern Recognition (CVPR)*, 2017. [2](#)
- [45] Eric Tzeng, Judy Hoffman, Ning Zhang, Kate Saenko, and Trevor Darrell. Deep domain confusion: Maximizing for domain invariance. *arXiv preprint arXiv:1412.3474*, 2014. [2](#)
- [46] Tuan-Hung Vu, Himalaya Jain, Maxime Bucher, Matthieu Cord, and Patrick Pérez. Dada: Depth-aware domain adaptation in semantic segmentation. In *Proceedings of the IEEE international conference on computer vision (ICCV)*, 2019. [1](#), [6](#)
- [47] Ting-Chun Wang, Ming-Yu Liu, Jun-Yan Zhu, Andrew Tao, Jan Kautz, and Bryan Catanzaro. High-resolution image synthesis and semantic manipulation with conditional gans. In *Proceedings of the IEEE Conference on Computer Vision and Pattern Recognition (CVPR)*, 2017. [5](#)
- [48] Zuxuan Wu, Xintong Han, Yen-Liang Lin, Mustafa Gokhan Uzunbas, Tom Goldstein, Ser Nam Lim, and Larry S Davis. Dcan: Dual channel-wise alignment networks for unsupervised scene adaptation. In *Proceedings of the European Conference on Computer Vision (ECCV)*, pages 518–534, 2018. [1](#), [2](#), [3](#)
- [49] Wei Ying, Yu Zhang, Junzhou Huang, and Qiang Yang. Transfer learning via learning to transfer. In *International Conference on Machine Learning (ICML)*, pages 5072–5081, 2018. [2](#)
- [50] Yang Zhang, Philip David, and Boqing Gong. Curriculum domain adaptation for semantic segmentation of urban scenes. In *Proceedings of the IEEE international conference on computer vision (ICCV)*, 2017. [1](#)
- [51] Yiheng Zhang, Zhaofan Qiu, Ting Yao, Dong Liu, and Tao Mei. Fully convolutional adaptation networks for semantic segmentation. In *Proceedings of the IEEE Conference on Computer Vision and Pattern Recognition (CVPR)*, pages 6810–6818, 2018. [1](#), [2](#), [3](#)
- [52] Hengshuang Zhao, Jianping Shi, Xiaojuan Qi, Xiaogang Wang, and Jiaya Jia. Pyramid scene parsing network. In *Proceedings of the IEEE Conference on Computer Vision and Pattern Recognition (CVPR)*, pages 2881–2890, 2017. [2](#)
- [53] Jun-Yan Zhu, Taesung Park, Phillip Isola, and Alexei A Efros. Unpaired image-to-image translation using cycle-consistent adversarial networks. In *Proceedings of the IEEE international conference on computer vision (ICCV)*, 2017. [1](#)

- [54] Xinge Zhu, Hui Zhou, Ceyuan Yang, Jianping Shi, and Dahua Lin. Penalizing top performers: Conservative loss for semantic segmentation adaptation. In *Proceedings of the European Conference on Computer Vision (ECCV)*, pages 568–583, 2018. [1](#)
- [55] Yang Zou, Zhiding Yu, BVK Vijaya Kumar, and Jinsong Wang. Unsupervised domain adaptation for semantic segmentation via class-balanced self-training. In *Proceedings of the European Conference on Computer Vision (ECCV)*, pages 297–313. Springer, 2018. [1](#)